Energies **2015**, *8*, 8594-8612; doi:10.3390/en8088594

OPEN ACCESS

energies

ISSN 1996-1073

www.mdpi.com/journal/energies

Article

A Real-Time Joint Estimator for Model Parameters and State of Charge of Lithium-Ion Batteries in Electric Vehicles

Jianping Gao [1], Yongzhi Zhang [2,3,*] and Hongwen He [2,3,*]

[1] College of Vehicle and Transportation Engineering, Henan University of Science and Technology, Luoyang 471023, China; E-Mail: gaojp_hn@126.com

[2] National Engineering Laboratory for Electric Vehicles, School of Mechanical Engineering, Beijing Institute of Technology, Beijing 100081, China

[3] Collaborative Innovation Center of Electric Vehicles in Beijing, Beijing Institute of Technology, Beijing 100081, China

* Authors to whom correspondence should be addressed;
E-Mails: Zhangyz0130@163.com (Y.Z.); hwhebit@bit.edu.cn (H.H.);
Tel./Fax: +86-10-6891-4842 (Y.Z. & H.H.).

Academic Editor: Omar Hegazy

Received: 30 April 2015 / Accepted: 4 August 2015 / Published: 12 August 2015

Abstract: Accurate state of charge (SoC) estimation of batteries plays an important role in promoting the commercialization of electric vehicles. The main work to be done in accurately determining battery SoC can be summarized in three parts. (1) In view of the model-based SoC estimation flow diagram, the *n*-order resistance-capacitance (RC) battery model is proposed and expected to accurately simulate the battery's major time-variable, nonlinear characteristics. Then, the mathematical equations for model parameter identification and SoC estimation of this model are constructed. (2) The Akaike information criterion is used to determine an optimal tradeoff between battery model complexity and prediction precision for the *n*-order RC battery model. Results from a comparative analysis show that the first-order RC battery model is thought to be the best based on the Akaike information criterion (AIC) values. (3) The real-time joint estimator for the model parameter and SoC is constructed, and the application based on two battery types indicates that the proposed SoC estimator is a closed-loop identification system where the model parameter identification and SoC estimation are corrected mutually, adaptively and simultaneously according to the observer values. The maximum SoC estimation error is less than 1% for both battery types, even against the inaccurate initial SoC.

Keywords: electric vehicles; lithium-ion battery; real-time; state of charge; *n*-order RC model; Akaike information criterion

1. Introduction

The battery is a bottleneck technology for electric vehicles (EVs). It is valuable both in theory and practical application to carry out research on the state estimation of batteries, which is very crucial to optimize the energy management, extend the cycling life, reduce the cost and safeguard the application of batteries in EVs. However, batteries, with their major time-variable, nonlinear characteristics, are further influenced by such random factors as driving loads, operation environment, *etc.*, in terms of application in EVs. Real-time, accurate estimation of their state of charge (SoC) is challenging [1–3].

An assortment of techniques has previously been reported to measure or estimate the SoC of the cells or battery packs, each having its relative merits, as reviewed by Xiong *et al.* [4]. Generally, the model-based SoC estimation method is able to combine different kinds of SoC estimation methods to avoid the shortcomings of each one [5–10]. Figure 1 is the model-based SoC estimation flow diagram: the battery models and the online data are stored in the memorizers and the real-time data on current, voltage and temperature are collected by the sensors, then the main key technologies are left as the three aspects shown in Figure 1 as ①, ②, ③.

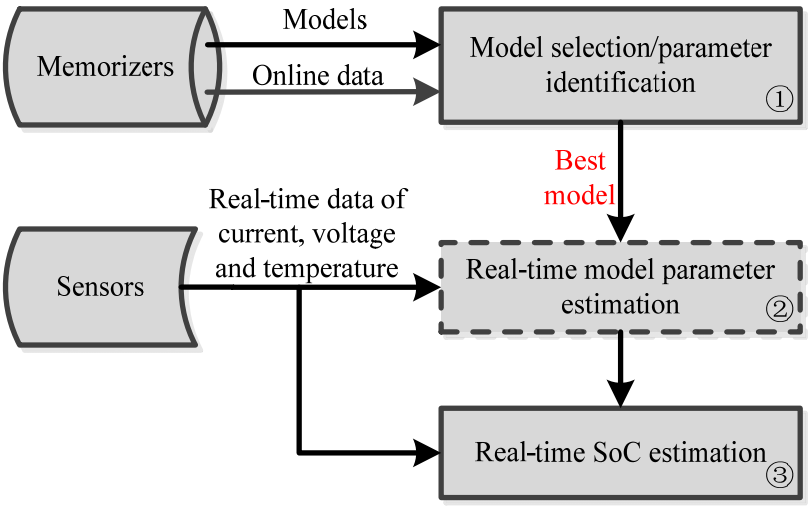

Figure 1. Model-based state of charge (SoC) estimation flow diagram.

For the first aspect, model selection/parameter identification, reference [7] summarized the battery models built in the National Renewable Energy Laboratory's advanced vehicle simulator, which include an internal resistance model, a resistance–capacitance model, the PNGV (partnership for new generation Of vehicles) model, a lead acid neural network model, a fundamental lead acid model, and Saber's lead acid electrical RC (resistance-capacitance) model; also the application limitations of these models are deeply researched and listed based on comparisons. Reference [11] proposes a generalized impedance-based model, which takes into account the non-homogeneous battery dynamics with nonlinear lumped elements. This model is verified to simulate the dynamic and transient response

of lithium-ion polymer batteries accurately by experimental results. Reference [12] uses the recursive least square method (RLS) to estimate the $LiFePO_4$ cell voltage and SoC online, and the results show that one or two RC networks connected to the Rint model in series are reasonable for the dynamic simulation of the $LiFePO_4$ battery module. Reference [13] takes the multi-swarm particle swarm optimization (MPSO) method to select the optimal model out of the twelve equivalent circuit models for the LiNMC cell and $LiFePO_4$ cell, and the results indicate that the first-order RC model is preferred for LiNMC cells, while the first-order RC model with one-state hysteresis seems to be the best choice for $LiFePO_4$ cells. Reference [14] takes six battery models into consideration and applies the least square method and extended Kalman filter (EKF) to identify the LiPB cell model parameters and estimate its voltage; the results indicate that the battery model accuracy could improve greatly with additional hysteresis and filter states at some cost in complexity, while it makes no sense to increase the filter state order beyond 4. In summary, it is difficult to build one unique battery model for all kinds of batteries with an acceptable accuracy. In addition, factors also influence the model selection process such as the dataset used, the model parameter identification method, the battery SoC estimation method, the model evaluation rule, and so on. However, we find that the *n*-order RC battery model is expected to simulate the characteristics of various kinds of batteries more accurately [11,12,15]. Usually model parameters can be identified during or after the model selection process.

For the second aspect, real-time model parameter identification, it is optional. In fact, the battery parameters change along with the battery application and aging. In online or even offline model parameter identification it is hard to accurately determine battery characteristics. Herein, it is necessary to identify the battery parameters in real-time. Based on the Thevenin battery model, reference [16] applies the moving window least square (LS) method to realize real-time model parameter identification, and a state observer is built to estimate the battery SoC simultaneously. However, in real applications it is difficult for the moving window LS to choose a reasonable parameter updating frequency to achieve stability because of the open-loop characteristic of the joint estimator. Reference [17] uses the adaptive joint EKF to identify a real-time model parameter which has a high order state-space equation by taking the model parameter as the state set. Besides, it is difficult to obtain accurate SoC just by the interpolation of the OCV (open circuit voltage)-SoC relationship based on the estimated OCV, especially for batteries with the flat OCV-SoC relationship. To tackle the problem caused by the flat OCV *vs*. SoC segments when the OCV-based SoC estimation method is adopted, reference [18] proposes a method combining the coulombic counting and the OCV-based method, where two different real-time model-based SoC estimation methods for Lithium-ion batteries are presented, one based on model parameter identification using the weighted RLS method and another based on state estimation using the EKF method.

For the third aspect, real-time SoC estimation, reference [19] implements the particle filter to estimate battery SoC, which is more accurate than EKF. However, the generation and operation of the numerous particles will create a heavy calculation burden in real applications. To reduce the calculation requirement, reference [20] proposes a new SoC estimation method based on a square root unscented Kalman filter using a spherical transform (Sqrt-UKFST) with unit hyper sphere. However, it still suffers from certain numerical stabilities. In contrast, the central difference Kalman filter (CDKF) is a stable algorithm and able to generate certain number of points for state estimation intelligently. References [21,22] indicate that CDKF, as one sigma-points Kalman filter (SPKF) method, is able to

avoid the linearization error of the battery model and improve the model's precision for SoC estimation, which has the potential to solve the nonlinear estimation problems [23–27].

1.1. Contribution of the Paper

In order to select the optimal battery model based on the measured data on current and voltage, the Akaike information criterion (AIC) is applied to make a tradeoff between battery prediction precision and complexity. Based on the selected battery model in different life stages, the input-output equation is built and the RLS algorithm is used to identify the model parameter in real time to track the time-varying characteristic of the battery. Also, the relationship between OCV and SoC is employed to describe the nonlinear characteristic of the battery, and to avoid the linearization error of the state-space equation for SoC estimation, the CDKF algorithm is applied to realize the real-time nonlinear SoC estimation. By combining the RLS and CDKF algorithms, the real-time closed-loop joint estimator for battery parameter and SoC is constructed.

1.2. Organization of the Paper

In order to estimate the parameters and SoC of a battery in real time, this paper is organized as follows: the battery modeling and real-time parameter identification process is described in Section 2. Then, the CDKF-based SoC estimator is constructed in Section 3. Section 4 shows the dataset of the lithium-ion cell for verification. Then, verification and discussion are in Section 5; Finally, some conclusions are made in Section 6.

2. Battery Modeling and Real-Time Parameter Identification

The *n*-order RC battery model is employed here to simulate the battery characteristics and the schematic diagram is shown in Figure 2, where i_L is the load current with a positive value in the discharge process and a negative value in the charge process; U_t is the terminal voltage; U_{OC} is the open circuit voltage (OCV); R_i is the equivalent ohmic resistance; C_i is the ith equivalent polarization capacitance and R_i is the ith equivalent polarization resistance simulating the transient response during a charge or discharge process; U_i is the voltage across C_i. $i = 1, 2, 3, \ldots, n$.

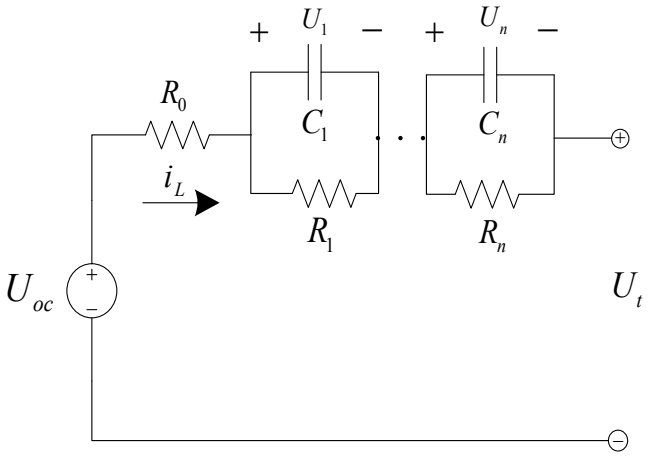

Figure 2. Schematic diagram of the *n*-order resistance-capacitance (RC) battery model.

According to reference [10], the *n*-order RC battery model is expressed as:

$$U_{t,k} - U_{oc,k} = \sum_{i=1}^{n} a_i \left(U_{t,k-i} - U_{oc,k-i} \right) + \sum_{i=0}^{n} b_i i_{L,i} \tag{1}$$

where a_i and b_i (i = 1, 2, 3, … , n) are the fitting coefficients and can be expressed as the functions of the battery model parameters.

The RLS method is applied to identify the model parameters in real time, and the identification process is as follows [10]:

$$\begin{cases} \theta_k = \left[a_1, a_2, ..., a_n, b_0, b_1, ..., b_n \right] \\ \phi_k = \left[U_{t,k-1} - U_{\mathrm{oc},k-1}, U_{t,k-2} - U_{\mathrm{oc},k-2}, \ldots, U_{t,k-n} - U_{\mathrm{oc},k-n}, i_{L,k}, i_{L,k-1}, \ldots, i_{L,k-n} \right] \\ K_{Ls,k} = P_{Ls,k-1} \phi_k^T \left[\phi_k P_{Ls,k-1} \phi_k^T + \mu \right]^{-1} \\ \hat{\theta}_k = \hat{\theta}_{k-1} + K_{Ls,k} \left[y_k - \phi_k \hat{\theta}_{k-1} \right] \\ P_{Ls,k} = \dfrac{1}{\mu} \left[I - K_{Ls,k} \phi_k \right] P_{Ls,k-1} \end{cases} \tag{2}$$

where $\hat{\theta}_k$ is estimate of the parameter vector θ_k; $K_{Ls,k}$ is the algorithm gain matrix and $P_{Ls,k}$ is the covariance matrix; the constant μ is the forgetting factor and is very important to obtain a good estimated parameter set with small error, typically $\mu \in [0.95,1]$. The reader is referred to reference [10] for the detailed mathematical model deduction and RLS-based model parameter identification process.

3. Central Difference Kalman Filter (CDKF)-Based State of Charge (SoC) Estimator

3.1. State of Charge Definition

In this study, battery SoC has been defined by the following Equation [28]:

$$z_k = z_{k-1} - \frac{\eta_k i_{L,k} \Delta t}{C_a} \tag{3}$$

where Δt represents the sampling time, C_a represents the available capacity of battery, and η denotes the current efficiency of battery.

3.2. State-Space Modeling

The state space equation of Figure 2 for SoC estimation is expressed as [28]:

$$\begin{cases} x_k = f\left(x_{k-1}, U_{t,k-1}, i_{L,k} \right) + \omega_{k-1} \\ y_k = h\left(x_k, U_{t,(k-1,\ldots,k-n)}, i_{L,(k,\ldots,k-n)} \right) + \upsilon_k \end{cases} \tag{4}$$

where

$$\begin{cases} x_k = \begin{bmatrix} U_{1,k} \\ \cdots \\ U_{n,k} \\ z_k \end{bmatrix}, y_k = U_{t,k} \\ f\left(x_{k-1}, U_{t,k-1}, i_{L,k}\right) = \begin{bmatrix} \exp\left(-\dfrac{\Delta t}{R_1 C_1}\right) & 0 & \cdots & 0 \\ \cdots & \cdots & \cdots & \cdots \\ 0 & \cdots & \exp\left(-\dfrac{\Delta t}{R_n C_n}\right) & 0 \\ 0 & \cdots & 0 & 1 \end{bmatrix} \begin{bmatrix} U_{1,k-1} \\ \cdots \\ U_{n,k-1} \\ z_{k-1} \end{bmatrix} + \begin{bmatrix} R_1\left[1-\exp\left(-\dfrac{\Delta t}{R_1 C_1}\right)\right] \\ \cdots \\ R_n\left[1-\exp\left(-\dfrac{\Delta t}{R_n C_n}\right)\right] \\ -\dfrac{\Delta t}{C_a} \end{bmatrix} i_{L,k} \\ h\left(x_k, U_{t,(k-1,\ldots,k-n)}, i_{L,(k,\ldots,k-n)}\right) = U_{oc}\left(z_k\right) - \sum_{i=1}^{n} U_{i,k} - R_0 i_{L,k} \end{cases} \tag{5}$$

$U_{oc}\left(z_k\right)$ is the OCV value obtained by the interpolation based on the OCV-SoC relationship, which represents the battery nonlinear characteristic. Both ω_k and υ_k are assumed unrelated white Gaussian random processes, with zero mean and covariance matrices with known value:

$$E\left[\omega_n \omega_k^T\right] = \begin{cases} Q_k, n = k; \\ 0, \quad n \neq k. \end{cases} \qquad E\left[\upsilon_n \upsilon_k^T\right] = \begin{cases} R_k, n = k; \\ 0, \quad n \neq k. \end{cases} \tag{6}$$

3.3. SoC Estimation Using the Central Difference Kalman Filter Algorithm

To deal with the battery's nonlinear characteristic, the CDKF algorithm is proposed to build the battery SoC estimator. The CDKF algorithm estimates the mean and covariance of the output of a non-linear function using a small fixed number of function evaluations. A set of points (sigma points) is obtained from the function so that the (possibly weighted) mean and covariance of the points exactly matches the mean and covariance of the *a priori* random variable being modeled. These points are then passed through the non-linear function, resulting in a transformed set of points. The *a posteriori* mean and covariance that are sought are then approximated by the mean and covariance of these points. It is noted that the CDKF algorithm can avoid the linearization error of the state-space equation. The reader is referred to reference [21] for the detailed calculation process of the CDKF algorithm.

Figure 3 shows the general diagram of the real-time joint SoC estimator and the operating steps are as follows:

- Data measurement. The sensors collect the real-time data on current, voltage and temperature at each sampling time, and then the collected data are applied to identify the model parameters and estimate the SoC real-timely.
- Model parameter identification. The RLS method is used to realize real-time model parameter identification based on the collected data of current and voltage. Then the identified model parameters are transferred to the CDKF-based SoC estimator and the estimated OCV value is transferred back in turn. Herein, a stable and accurate RLS-based model parameter

identification process can ensure, and at the same time is based on the good stability and high accuracy of the CDKF estimator.

- CDKF-based SoC estimator. The CDKF algorithm is used to estimate the SoC based on the identified model parameters. In this process, if model parameters are not identified correctly, the CDKF estimator will not work normally, thus leading to the wrong returned OCV value. However, the RLS and CDKF automatically correct the wrong estimates based on the big observer errors and gain matrices simultaneously, then both estimates of them will converge to the true values quickly, which realizes the close-loop SoC estimation process. Herein the proposed estimator in this paper is able to estimate the SoC accurately against different operating environment disturbances.

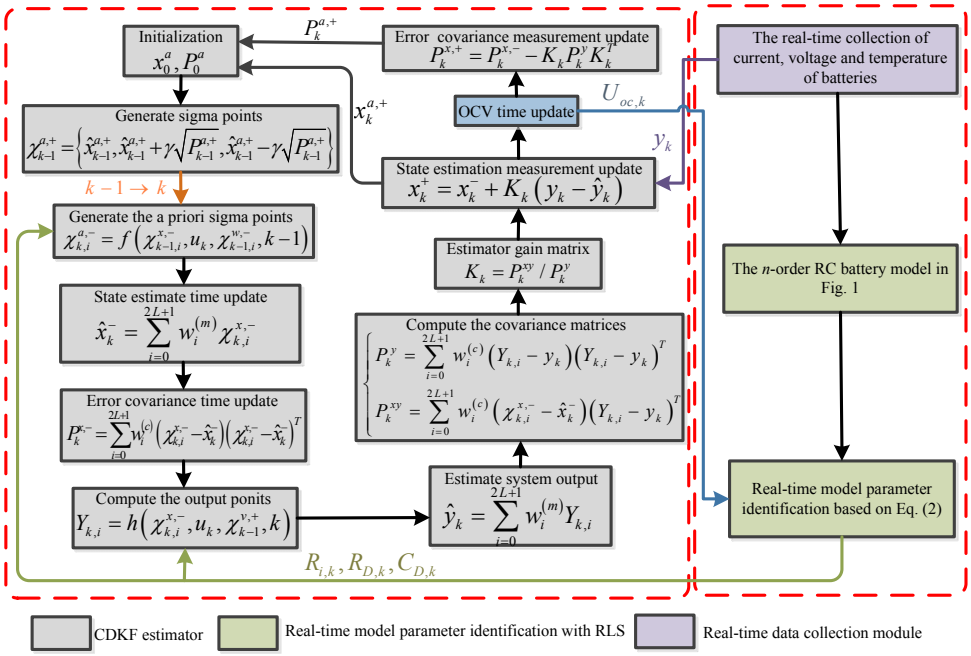

Figure 3. The general diagram of the real-time joint SoC estimator.

4. Data Set of Lithium-Ion Cell for Verification

4.1. Experiment Setup

As a verification case, the $LiFePO_4$ cell and $LiMn_2O_4$ cell are selected to evaluate the proposed method.

The test bench setup is shown in Figure 4. It is made up of an Arbin BT2000 battery cycler (Arbin company, College Station TX, USA), a thermal chamber used to control the operation temperature, a computer used to do programming and store experimental data and one $LiFePO_4$/$LiMn_2O_4$ cell. The battery cycler channel is applied to load the current or power profiles on the test cells with the voltage range of 0–60 V and current range of ±300 A, and its recorded data include current, voltage, temperature, charge-discharge amp-hours (Ah), watt-hours (Wh), *etc.* The measurement error of the current and voltage sensors inside the Arbin BT2000 cycler is less than ±0.05%. The measured data is passed to the host computer through TCP/IP ports. The test cell is connected with the Arbin BT2000 cycler and then placed inside the thermal chamber to maintain the desired temperatures to perform special behavior.

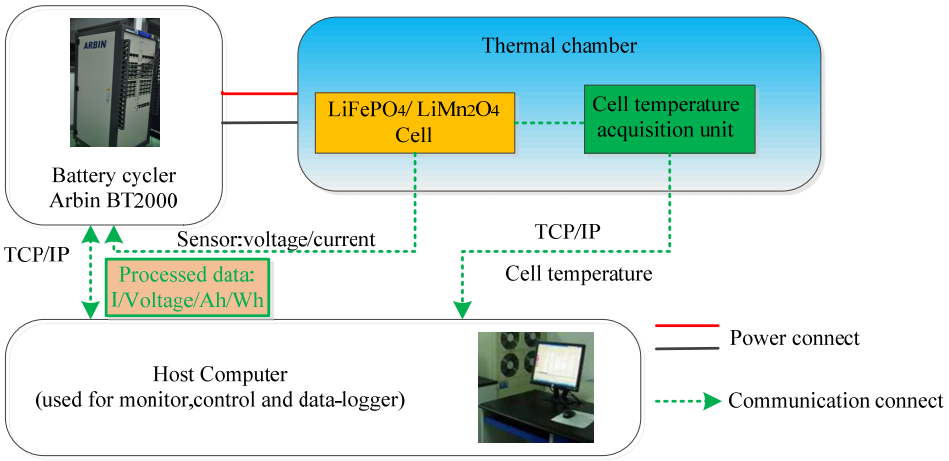

Figure 4. The battery test bench.

4.2. Battery Test

The characteristics of the two types of batteries used are shown in Table 1. From Table 1 we can see that the $LiFePO_4$ cell capacity has decreased about 4.35% and the $LiMn_2O_4$ cell capacity has decreased about 9.11%. The experimental data used in this paper are respectively shown in Figures 5–9. It is important to note that in this research, we only consider the operation temperature at 25 °C.

Table 1. Main specifications of the two types of batteries.

Lithium-Ion Battery Cell	$LiFePO_4$	$LiMn_2O_4$
Nominal capacity (Ah)	2.3	35
Maximum available capacity (Ah)	2.2	31.81
Nominal voltage (V)	3.3	3.7
Upper cut-off voltage (V)	3.8	4.2
Lower cut-off voltage (V)	1.6	3.0

Figures 5–7 show the experimental data of the $LiFePO_4$ cell. Figure 5 is the relationship between battery SoC and OCV. Figure 6 shows the details of the hybrid pulse power characteristic (HPPC) test [29]. Figure 6a is the current profile, and Figure 6b is the voltage profile. Figure 6c,d describes a sample HPPC current curve and voltage curve, respectively. The profiles of the Dynamic Stress Test (DST) are shown in Figure 7. Figure 7a describes the experimental current. Figure 7b is the terminal voltage, and Figure 7c describes the calculated SoC. The sample frequency is set to 1 Hz.

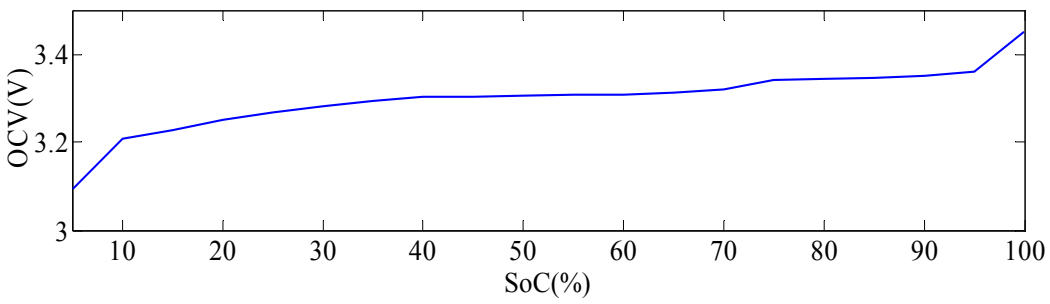

Figure 5. SoC *vs*. OCV (open circuit voltage) of the $LiFePO_4$ cell.

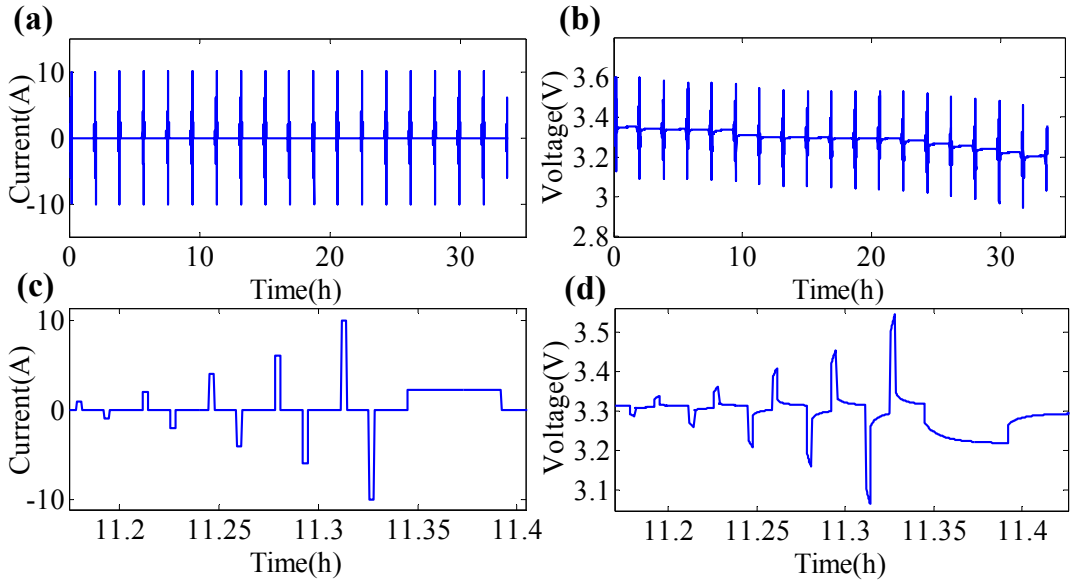

Figure 6. The hybrid pulse power characteristic HPPC (hybrid pulse power characteristic) test of the $LiFePO_4$ cell: (**a**) Current; (**b**) Voltage; (**c**) One current profile; (**d**) One voltage profile.

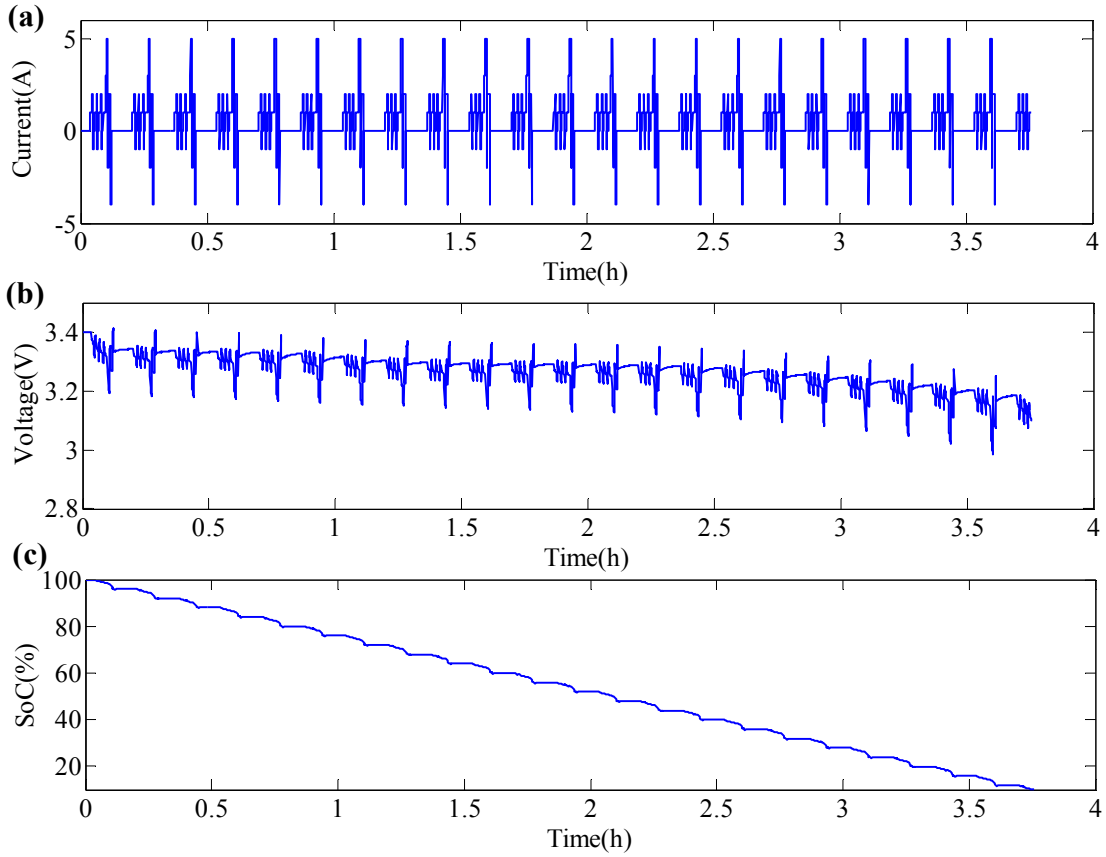

Figure 7. The dynamic stress test of the $LiFePO_4$ cell: (**a**) Current; (**b**) Voltage; (**c**) SoC.

Figures 8 and 9 show the experimental data of the $LiMn_2O_4$ cell. Figure 8 is the relationship between battery SoC and OCV. The profiles of the Beijing Driving cycles (BJDC) are shown in Figure 9. Figure 9a describes the experimental current. Figure 9b is the terminal voltage, and Figure 9c describes the calculated SoC. The sample frequency is set to 1 Hz.

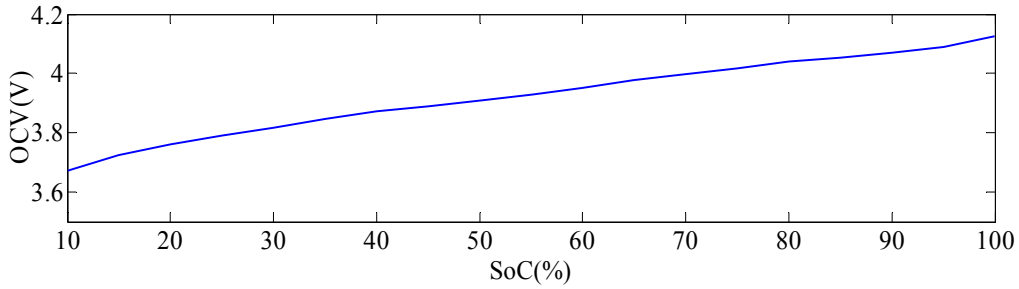

Figure 8. SoC *vs*. OCV of the $LiMn_2O_4$ cell.

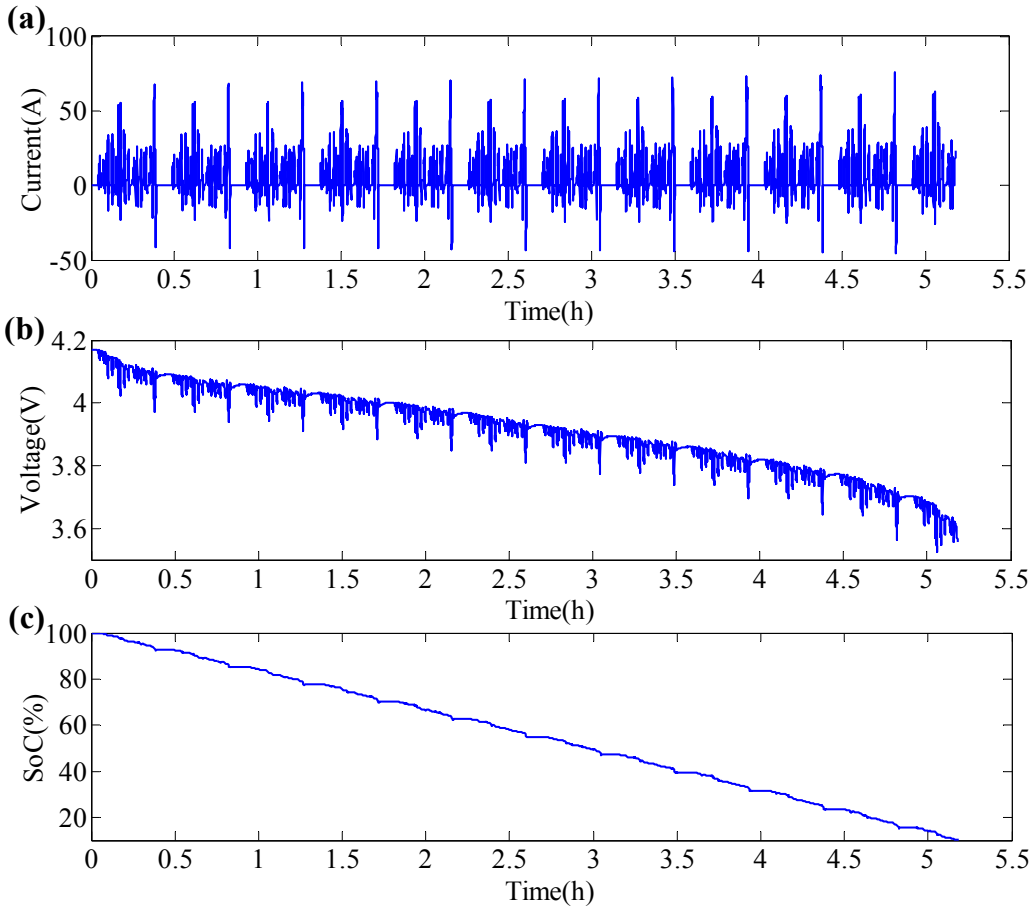

Figure 9. The Beijing Driving cycles (BJDC) test of the $LiMn_2O_4$ cell: (**a**) current; (**b**) voltage; (**c**) SoC.

5. Verification and Discussion

Considering practical applications, only the portion of the test data within 10%–90% SoC in these datasets is used in SoC estimation.

5.1. Model Selection

Referring to the *n*-order RC battery model, Reference [12] points out the model parameters will increase abundantly with the increase of the number of RC networks, and the calculation burden will be heavier and a larger memory will be required to store the large amount of sample data. It is meaningful to properly select a minimum RC network with an acceptable accuracy.

In this paper the AIC is employed to establish a tradeoff between the model complexity and prediction precision. The information-theoretic or entropic AIC criterion aims to identify an optimal and parsimonious model in data analysis from a class of competing models which takes model complexity into account [30].The AIC model used here is as:

$$\mathrm{AIC} = 2\log \hat{s}_k^2 + 2n \tag{7}$$

where n denotes the RC order of the combined model. $\hat{s}_k^2$ denotes the sum of the residual error squares based on the RLS method (Equation (2)) and is expressed as:

$$\hat{s}_k^2 = \frac{1}{N}\sum_{k=1}^{N}\left(y_k - \hat{y}_k\right)^2 \tag{8}$$

where N denotes the data length.

The datasets used here are the HPPC profiles of the $LiFePO_4$ cell. Figure 10 plots the model voltage prediction errors with $n = 0 - 5$, and the statistical results are shown in Table 2. From Table 2, we can see that the minimum AIC value is −4.80 if n equals 1. When n equals 0, the battery model is simple but the model precision is poor. From Table 2 we can see that the maximum voltage prediction error is up to 67.02 mV, while the model precision mainly operates on calculating the AIC which is then large. From Figure 10 we can see that the voltage prediction precision improves greatly if n increases to 1 from 0, and Table 2 shows that the maximum voltage error decreases about 60 mV, thus leading to the decrease of AIC. However, from Figure 10 and Table 2 we can see that the model precision improves only a little as n continues to increase; for example the standard deviation decreases only 0.05 mV if n increases to 5 from 1, and the maximum voltage error is even worse during this process, while the model complexity mainly operates on calculating the AIC. Herein the AIC value will continue to increase with the increase of n from 1.

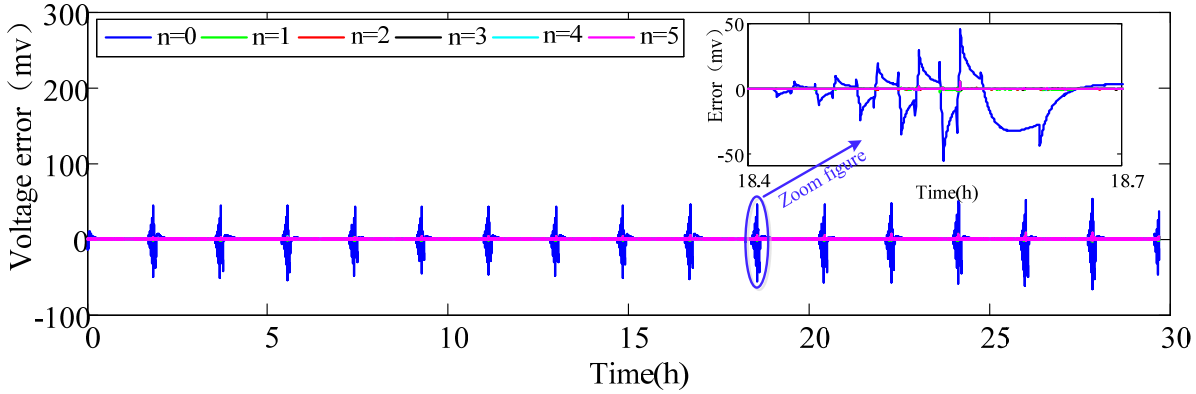

Figure 10. Model voltage prediction error with n = 0–5.

Hence the model with n = 1 is the optimal tradeoff between the model complexity and precision, which is thus selected to implement the SoC estimation later. The duration of each case is also shown in Table 2. Note that all the procedures in this paper are run in Matlab/Simulink R2012b version with the HP Z620 workstation (Hewlett-Packard Development Company, Palo Alto, CA, USA) equipped with an Intel Xeon E5-2620 v2@2.10GHz CPU and 32 GB of RAM.

Table 2. Statistical results of voltage prediction error.

n	Maximum (mV)	Mean (mV)	Standard Deviation (mV)	AIC	Duration (s)
0	67.02	−0.30	6.02	7.18	4.64
1	7.68	7.9×10^{-3}	0.18	−4.80	4.75
2	8.82	9.3×10^{-3}	0.15	−3.67	4.93
3	8.81	7.2×10^{-3}	0.14	−1.93	5.28
4	8.77	5.7×10^{-3}	0.13	−0.04	5.54
5	8.74	4.4×10^{-3}	0.13	1.88	5.90

5.2. SoC Estimation

The datasets firstly used here are the DST profiles of the $LiFePO_4$ cell, which are regarded as the real-time data to drive the CDKF-based SoC estimator. It is noted that the exact initial SoC is 90%. Also, an inaccurate initial SoC of being 80% is set to evaluate the robustness of the proposed estimator.

Figure 11 is the model parameter identification results with different initial SoCs of the $LiFePO_4$ cell. Figure 11a is the internal resistance R_0. Figure 11b is the polarization resistance R_1 and Figure 11c is the polarization capacitance C_1. From Figure 11 we find that the estimation results of the 80% initial SoC case are the same with that of the 90% initial SoC case, which is in accordance with the real applications. Besides, the model parameters converge to the true values quickly after the initial fluctuation. We also find that as the SoC decreases the R_0 increases gently, but the R_1 and C_1 both change strongly. This is because the polarization resistance and capacitance describe the transient characteristic of battery which varies greatly when the battery is in charge or discharge, while the internal resistance does not.

Figure 12 is the voltage prediction results with different initial SoCs of the $LiFePO_4$ cell based on the identified model parameters. Figure 12a describes the reference terminal voltage and the predicted terminal voltage. Figure 12b describes the voltage prediction error. Statistical results of the voltage prediction error are shown in Table 3. From Figure 12 and Table 3 we find that the predicted voltage agrees very well with the reference voltage and the maximum predicted voltage error is less than 5 mV for both cases of initial SoCs being respectively 90% and 80%.

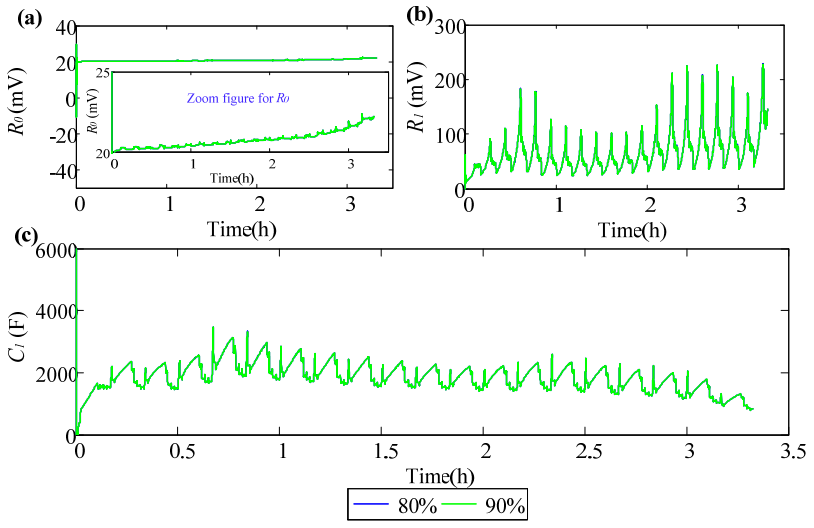

Figure 11. Model parameter identification results of the $LiFePO_4$ cell: (**a**) R_0; (**b**) R_1; (**c**) C_1.

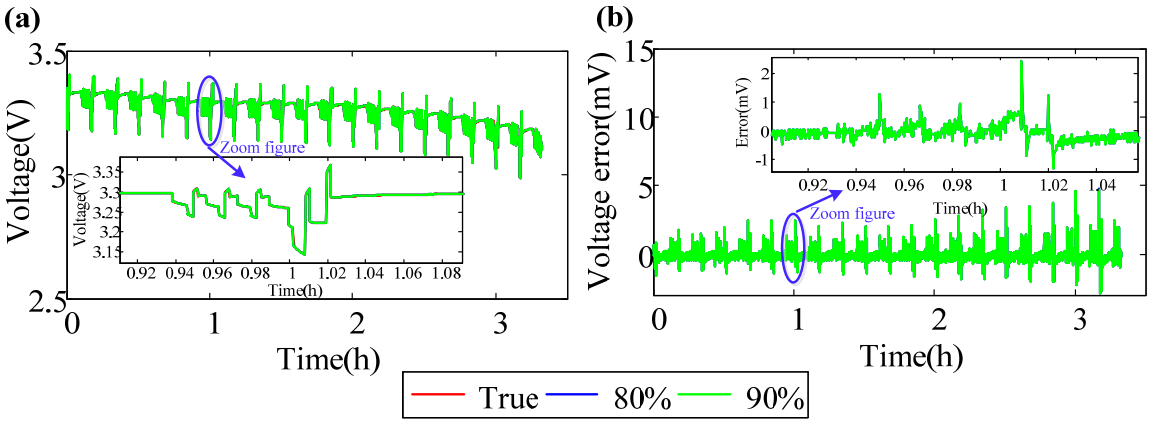

Figure 12. Voltage prediction results of the $LiFePO_4$ cell: (**a**) voltage; (**b**) voltage error.

Table 3. Statistical results of the voltage prediction error.

Initial SoC (%)	Maximum (mV)	Mean (mV)	Standard Deviation (mV)
90%	4.71	-8.42×10^{-2}	3.56×10^{-2}
80%	4.72	-8.43×10^{-2}	3.56×10^{-2}

Figure 13 describes the SoC estimation results, where the initial SoC value is set at the exact 90%.

It is noted that, in all cases, SoC reference profiles are calculated from the Arbin data-logger using power counting on measured data. In order to get the reference SoC profiles, the cells are firstly fully charged and lastly fully discharged after several loading profiles test with nominal current. In this way, we can get accurate initial SoC and terminal SoC. Then, the SoC reference trajectory is achieved based on the Arbin data-logger and the correction from the current efficiency map. In most cases, the battery's current efficiency is close to 100%.

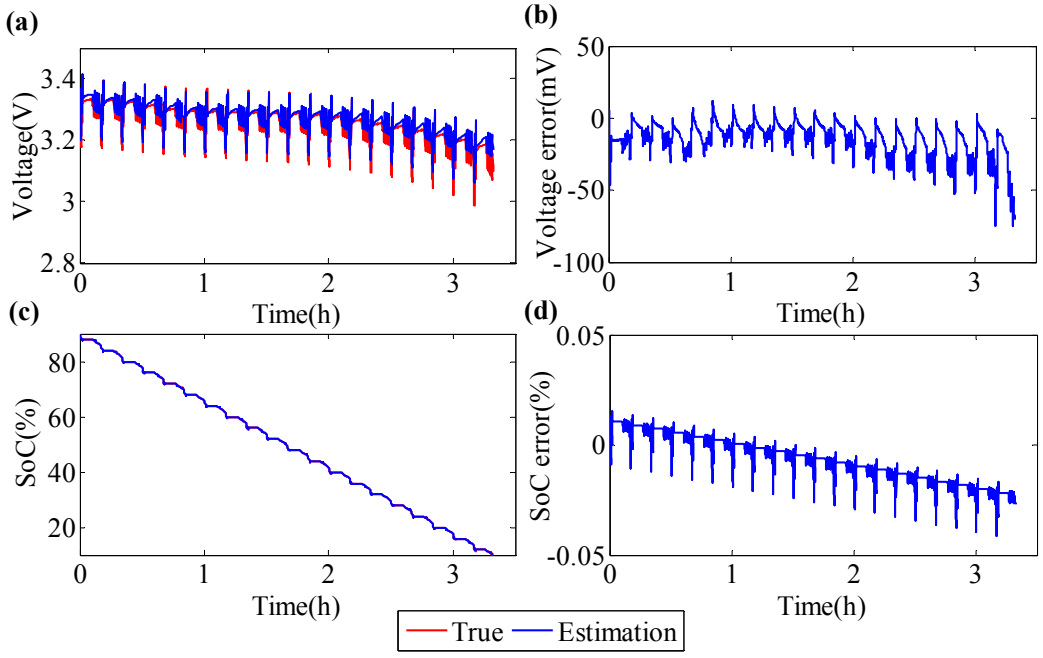

Figure 13. SoC estimation results with the accurate initial SoC of the $LiFePO_4$ cell: (**a**) Voltage; (**b**) Voltage error; (**c**) SoC; (**d**) SoC error.

The SoC estimation results with the accurate initial SoC of the $LiFePO_4$ cell are shown in Figure 13. Figure 13a describes the reference terminal voltage and the estimated terminal voltage. Figure 13b shows the voltage estimation error. The reference SoC and the estimated SoC are shown in Figure 13c. Figure 13d describes the SoC estimation error. It is noted that the accurate CDKF-based SoC estimation depends on the accurate RLS-based model parameter identification, and the return of the accurate OCV will further ensure the high estimation accuracy of the RLS algorithm. From Figure 13a,b we find that the voltage estimation result is good, and Table 4 shows that the voltage mean error and standard deviation are respectively −14.30 and 11.32 mV. However, if the more accurate estimated voltage is needed, we can always apply the RLS-based voltage estimation in real applications. From Figure 13c,d we find that the SoC estimation is very accurate, and Table 4 shows that the maximum SoC estimation error is only 0.04%. In considering that the model parameters are identified in real time based on the RLS algorithm, the CDKF-based SoC estimator is expected to realize the accurate voltage and SoC estimation against different operation conditions. Table 4 also shows the joint estimation duration in this case, which is 48.585 s. Compared to the duration in Table 2 we find that the calculation complexity will be much heavier if the dual-CDKF joint estimator is constructed referring to reference [18].

Table 4. Statistical results of the SoC estimation error.

Index	Maximum	Mean	Standard Deviation	Duration (s)
SoC (%)	0.04	−0.01	0.01	48.585
Voltage (mV)	74.63	−14.30	11.32	

However, during practical applications the accurate initial SoC value cannot be obtained, so the robustness of the SoC estimator against inaccurate initial values should be systematically studied. Figure 14 and Table 5 show the SoC estimation results with an inaccurate initial SoC, where the initial SoC is incorrectly set to 80%.

Figure 14 describes the SoC estimation results with an inaccurate initial SoC of the $LiFePO_4$ cell. Figure 14a describes the reference voltage and the estimated voltage. Figure 14b shows the estimated voltage error. Figure 14c describes the reference SoC and SoC estimation, and Figure 14d shows the SoC estimation error. The statistical results of the SoC estimation are listed in Table 5. From Figure 14, we find that the estimated terminal voltage and SoC are converged to the reference trajectory quickly after only one second for correcting the erroneous initial state of the SoC estimator. This is because the proposed estimator can precisely estimate the voltage and adjust the Kalman gain according to the terminal voltage error between the true values and the estimated values timely. The erroneous SoC estimation brings bigger terminal voltage errors, which will in turn produce a large Kalman gain matrix and then compensate the SoC estimation in efficient closed-loop feedback. Thus it can achieve the accurate SoC estimates, especially with a significant SoC offset. From Table 5 we find that the maximum SoC estimation error is only 0.05% after the inaccurate initial SoC converges with the reference value. The joint estimation duration is 49.115 s when the inaccurate initial SoC is set to 80%.

Thus the joint estimator is able to describe the $LiFePO_4$ cell characteristics accurately and realize the precise real-time battery parameter and SoC estimation even when the cell capacity decreases about 4.35%.

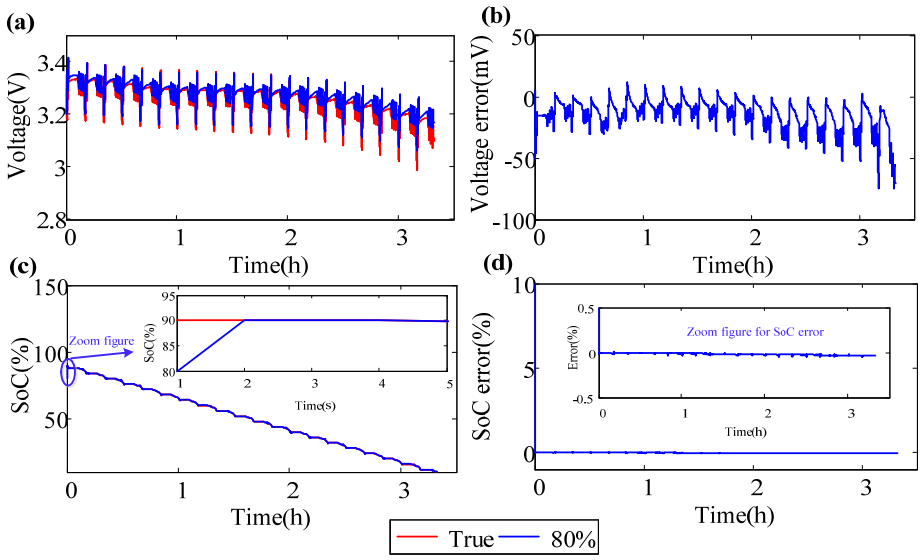

Figure 14. SoC estimation results with an inaccurate initial SoC (SoC_0 = 80%) of the $LiFePO_4$ cell: (**a**) voltage; (**b**) voltage error; (**c**) SoC; (**d**) SoC error.

Table 5. Statistical results of the SoC estimation error.

Index	Maximum	Mean	Standard Deviation	Duration (s)
SoC (%)	0.05	−0.02	0.01	49.115
Voltage (mV)	74.67	−14.31	11.32	

In order to further verify the proposed SoC estimator against different battery types, the BJDC datasets of the $LiMn_2O_4$ cell are used. It is noted the exact initial SoC is 90%.

Figure 15 is the model parameter identification results with different initial SoCs of the $LiMn_2O_4$ cell. Figure 15a is the internal resistance R_0. Figure 15b is the polarization resistance R_1 and Figure 15c is the polarization capacitance C_1. Still, as the results show in Figure 11, the estimation results of the 80% initial SoC case are the same with that of the 90% initial SoC case. Also, the model parameters converge to the true value quickly, and compared to the internal resistance, the polarization resistance and capacitance fluctuates more strongly.

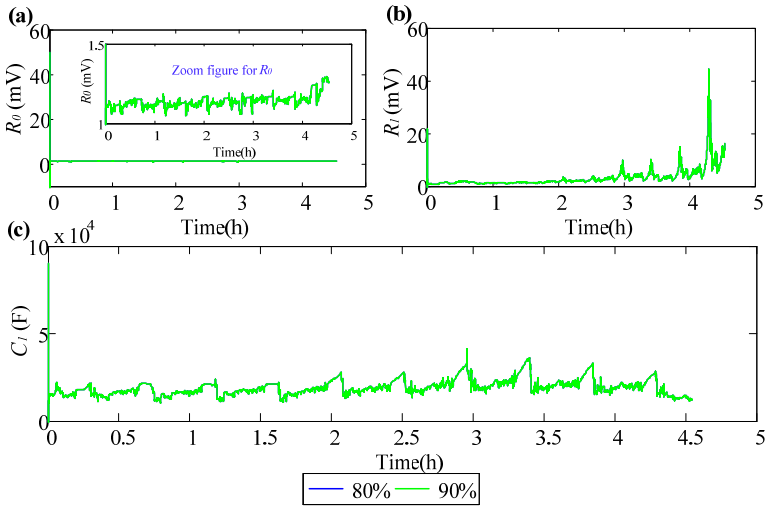

Figure 15. Model parameter identification results of the $LiMn_2O_4$ cell: (**a**) R_0; (**b**) R_1; (**c**) C_1.

Figure 16 describes the voltage prediction results with different initial SoCs of the $LiMn_2O_4$ cell. Figure 16a shows the reference voltage and the predicted voltage, and Figure 16b shows the voltage prediction error. The statistical results of the voltage prediction error are presented in Table 6. Still from Figure 16 and Table 6, we find that the RLS-based predicted voltage is very accurate, with the maximum estimation error being within 7 mV for both cases.

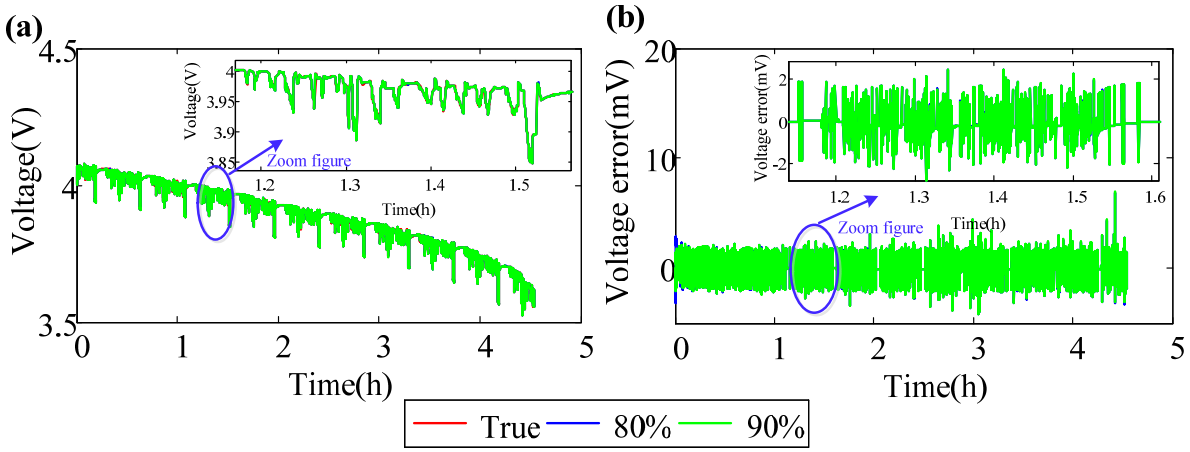

Figure 16. The voltage prediction results of the $LiMn_2O_4$ cell: (**a**) Voltage; (**b**) Voltage error.

Table 6. Statistical results of the voltage prediction error.

Initial SoC (%)	Maximum (mV)	Mean (mV)	Standard (mV)
90%	6.95	-8.16×10^{-2}	0.74
80%	6.85	-8.58×10^{-2}	0.74

Figure 17 shows the SoC estimation results with different initial SoCs of the $LiMn_2O_4$ cell, where the initial SoCs are respectively set to 80% and 90%. Figure 17a describes the reference voltage and the estimated voltage and Figure 17b describes the voltage estimation error. Figure 17c shows the reference SoC and the estimated SoC, and Figure 17d describes the SoC estimation error. The statistical results of the SoC estimation are listed in Table 7. From Figure 17 we find that for the case of the initial SoC being 80%, the estimated terminal voltage and SoC converged with the reference trajectory quickly after only one second for correcting the erroneous initial state of the SoC estimator. Afterwards, it traces the reference SoC trajectory stably and accurately just like the exact initial SoC case does. Table 7 shows that the maximum SoC estimation error is less than 1% for both cases. The voltage estimation result may not be as good as enough, still in real applications we can apply the RLS-based estimated voltage. The simulation durations of two cases are also shown in Table 7. Herein, the joint estimator is able to describe the $LiMn_2O_4$ cell characteristics accurately and realize the precise real-time battery parameter and SoC estimation even when the cell capacity decreases about 9.11%.

Table 7. Statistical results of the SoC estimation error.

Initial SOC (%)	Voltage Prediction Error (mV)			SOC Estimation Error (%)			Duration (s)
	Maximum	Mean	Standard Deviation	Maximum	Mean	Standard Deviation	
80	73.98	−4.83	9.29	0.77	−0.28	0.23	63.017
90	72.93	−4.89	9.36	0.65	−0.40	0.21	62.900

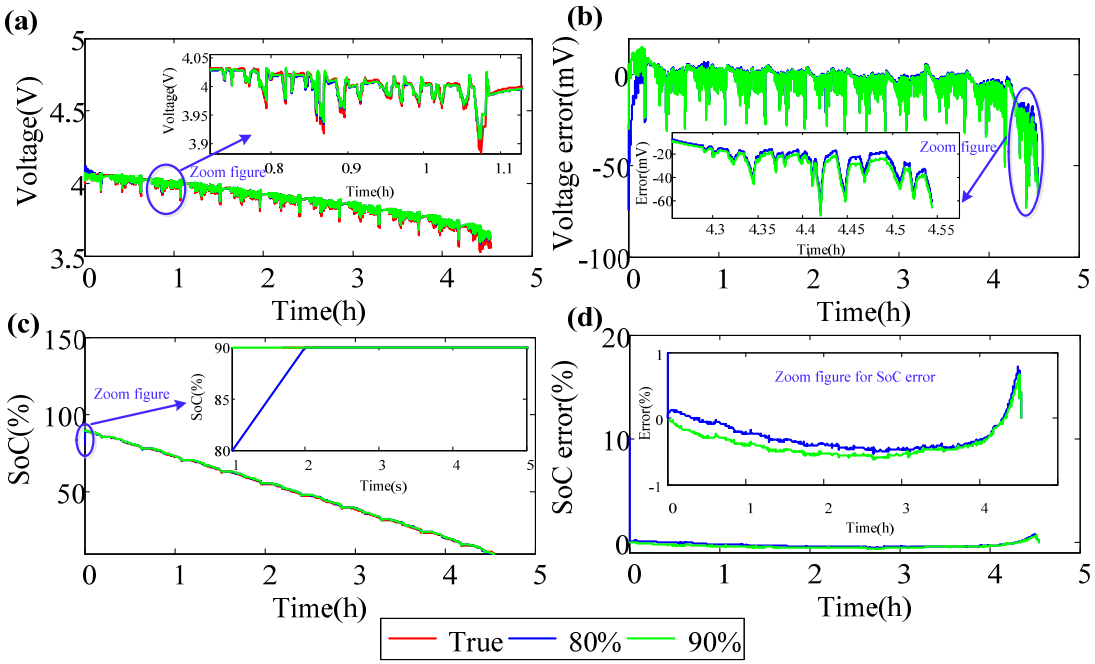

Figure 17. SoC estimation results with different initial SoCs of the $LiMn_2O_4$ cell: (**a**) Voltage; (**b**) Voltage error; (**c**) SoC; (**d**) SoC error.

6. Conclusions

In view of the model-based SoC estimation schematic diagram, the *n*-order RC battery model is proposed to simulate the major time-variable, nonlinear characteristics of batteries. To select a reasonable *n*, the AIC criterion is applied to establish the optimal tradeoff between the model complexity and prediction precision, and the results show that the first-order RC model is the best.

Then, a real-time joint estimator based on the RLS and CDKF algorithms is built to realize real-time battery model parameter identification and SoC estimation. The results based on the $LiFePO_4$ cell and the $LiMn_2O_4$ cell indicate that the proposed SoC estimator is a closed-loop identification system where the model parameter identification and SoC estimation are corrected mutually, adaptively and simultaneously according to the observer values. The maximum voltage prediction error is within 10 mV and the maximum SoC estimation error is less than 1%, even against an erroneous initial SoC. It is noted that the $LiFePO_4$ cell and the $LiMn_2O_4$ cell are in different life stages. Herein the proposed SoC estimator is expected to estimate SoC accurately even under different application and battery aging conditions.

Author Contributions

Jianping Gao contributed to the paper writing work and built the battery model. Yongzhi Zhang contributed to the paper writing work and did the SoC estimation. Hongwen He contributed to the paper writing work and provided the estimation algorithm.

Conflicts of Interest

The authors declare no conflict of interest.

Abbreviations

SoC: State of charge
AIC: Akaike information criterion
PNGV: Partnership for New Generation Of Vehicles
RC: Resistance-capacitance
OCV: Open circuit voltage
CDKF: Central difference Kalman filter
HPPC: Hybrid pulse power characteristic
DST: Dynamic Stress Test
BJDC: Beijing Driving cycles

References

1. Scrosati, B.; Garche, J. Lithium batteries: Status, prospects and future. *J. Power Sources* **2010**, *195*, 2419–2430.
2. Rydh, C.J.; Sandén, B.A. Energy analysis of batteries in photovoltaic systems. Part I: Performance and energy requirements. *Energy Convers. Manag.* **2005**, *46*, 1957–1979.
3. Shao, S.; Bi, J.; Yang, F.; Guan, W. On-line estimation of state-of-charge of Li-ion batteries in electric vehicle using the resampling particle filter. *Transp. Res. D Transp. Environ.* **2014**, *32*, 207–217.
4. Xiong, R.; He, H.; Sun, F.; Liu, X.; Liu, Z. Model-based state of charge and peak power capability joint estimation of lithium-ion battery in plug-in hybrid electric vehicles. *J. Power Sources* **2013**, *229*, 159–169.
5. Vasebi, A.; Partovibakhsh, M.; Bathaee, S.M.T. A novel combined battery model for state-of-charge estimation in lead-acid batteries based on extended Kalman filter for hybrid electric vehicle applications. *J. Power Sources* **2007**, *174*, 30–40.
6. ThermoAnalytics Inc. Battery Modeling for HEV Simulation by Thermo-Analytics Inc. Available online: http://www.thermoanalytics.com/support/publications/batterymodelsdoc.html (accessed on 7 August 2015).
7. Johnson, V.H. Battery performance models in ADVISOR. *J. Power Sources* **2002**, *110*, 321–329.
8. Liaw, B.Y.; Nagasubramanian, G.; Jungst, R.G.; Doughty, D.H. Modeling of lithium ion cells—A simple equivalent-circuit model approach. *Solid State Ionics* **2004**, *175*, 835–839.
9. Dubarry, M.; Vuillaume, N.; Liaw, B.Y. From single cell model to battery pack simulation for Li-ion batteries. *J. Power Sources* **2009**, *186*, 500–507.
10. Hu, Y.; Yurkovich, S.; Guezennec, Y.; Yurkovich, B.J. A technique for dynamic battery model identification in automotive applications using linear parameter varying structures. *Control Eng. Pract.* **2009**, *17*, 1190–1201.
11. Moss, P.L.; Au, G.; Plichta, E.J.; Zheng, J.P. An electrical circuit for modeling the dynamic response of Li-ion polymer batteries. *J. Electrochem. Soc.* **2008**, *155*, A986–A994.
12. He, H.; Zhang, X.; Xiong, R.; Xu, Y.; Guo, H. Online model-based estimation of state-of-charge and open-circuit voltage of lithium-ion batteries in electric vehicles. *Energy* **2012**, *39*, 310–318.
13. Hu, X.S.; Li, S.B.; Peng, H. A comparative study of equivalent circuit models for Li-ion batteries. *J. Power Sources* **2012**, *198*, 359–367.

14. Plett, G.L. Extended Kalman filtering for battery management systems of LiPB-based HEV battery packs: Part 2. Modeling and identification. *J. Power Sources* **2004**, *134*, 262–276.
15. He, H.W.; Xiong, R.; Fan, J.X. Evaluation of lithium-ion battery equivalent circuit models for state of charge estimation by an experimental approach. *Energies* **2011**, *4*, 582–598.
16. Rahimi-Eichi, H.; Baronti, F.; Chow, M.-Y. Online adaptive parameter identification and state-of-charge coestimation for lithium-polymer battery cells. *IEEE Trans. Ind. Electron.* **2014**, *61*, 2053–2061.
17. Feng, F.; Lu, R.G.; Wei, G.; Zhu, C.B. Online estimation of model parameters and state of charge of $LiFePO_4$ batteries using a novel open-circuit voltage at various ambient temperatures. *Energies* **2015**, *8*, 2950–2976.
18. Zhang, C.; Li, K.; Pei, L.; Zhu, C.B. An integrated approach for real-time model-based state-of-charge estimation of lithium-ion batteries. *J. Power Sources* **2015**, *283*, 24–36.
19. Wang, Y.J.; Zhang, C.B.; Chen, Z.H. A method for state-of-charge estimation of $LiFePO_4$ batteries at dynamic currents and temperatures using particle filter. *J. Power Sources* **2015**, *279*, 306–311.
20. Aung, H.; Low, K.S.; Goh, S.T. State-of-charge estimation of lithium-ion battery using square root spherical unscented Kalman filter (Sqrt-UKFST) in Nanosatellite. *IEEE Trans. Power Electron.* **2015**, *30*, 4774–4783.
21. Plett, G.L. Sigma-point Kalman filtering for battery management systems of LiPB-based HEV battery packs: Part 1: Introduction and state estimation. *J. Power Sources* **2006**, *161*, 1356–1368.
22. Plett, G.L. Sigma-point Kalman filtering for battery management systems of LiPB-based HEV battery packs: Part 2: Simultaneous state and parameter estimation. *J. Power Sources* **2006**, *161*, 1369–1384.
23. He, H.; Qin, H.; Sun, X.; Shui, Y. Comparison study on the battery SoC estimation with EKF and UKF algorithms. *Energies* **2013**, *6*, 5088–5100.
24. Li, J.; Barillas, J.K.; Guenther, C.; Danzer, M.A. A comparative study of state of charge estimation algorithms for $LiFePO_4$ batteries used in electric vehicles. *J. Power Sources* **2013**, *230*, 244–250.
25. Seo, B.H.; Nguyen, T.H.; Lee, D.C.; Lee, K.B.; Kim, J.M. Condition monitoring of lithium polymer batteries based on a sigma-point Kalman filter. *J. Power Electron* **2012**, *12*, 778–786.
26. Rigatos, G.G. Nonlinear Kalman filters and particle filters for integrated navigation of unmanned aerial vehicles. *Robot. Auton. Syst.* **2012**, *60*, 978–995.
27. Jaechan, L. CDKF approach for estimating a static parameter of carrier frequency offset based on nonlinear measurement equations in OFDM systems. *Nonlinear Dyn.* **2014**, *78*, 703–711.
28. Xiong, R.; Sun, F.; Gong, X.; He, H. Adaptive state of charge estimator for lithium-ion cells series battery pack in electric vehicles. *J. Power Sources* **2013**, *242*, 699–713.
29. Omar, N.; Daowd, M.; Bossche, P.V.D.; Hegazy, O.; Smekens, J.; Coosemans, T.; Mierlo, J.V. Rechargeable energy storage systems for plug-in hybrid electric vehicles—Assessment of electrical characteristics. *Energies* **2012**, *5*, 2952–2988.
30. Hendrik, K.; Robinson, K.; Philipp, S. *A Simple Specification Procedure for the Transition Function in Persistent Nonlinear Time Series Models*; Springer: Berlin, Germany, 2014.